Journal of Computational Physics 229 (2010) 221–232

Contents lists available at ScienceDirect

Journal of Computational Physics

journal homepage: www.elsevier.com/locate/jcp

Short Note

On the dissipation mechanism of upwind-schemes in the low Mach number regime: A comparison between Roe and HLL

Felix Rieper

Institut für Atmosphäre und Umwelt, Goethe-Universität Frankfurt, Altenhöferallee 1, D-60438 Frankfurt am Main, Germany

ARTICLE INFO

Article history:
Received 27 July 2009
Received in revised form 25 September 2009
Accepted 30 September 2009
Available online 12 October 2009

PACS:
47.11.Df
47.11.−j
47.15.G−
47.15.km

Keywords:
Incompressible and compressible flow
Euler equations
Low Mach number flow
Roe scheme
HLL
Numerical dissipation
Asymptotic analysis

ABSTRACT

It is well known that standard upwind schemes for the Euler equations face a number of problems in the low Mach number regime: stiffness, cancellation and accuracy problems. A new aspect of the *accuracy problem*, presented in this paper, is the dependence on the type of flux solver: while the accuracy of the HLL scheme massively decreases for $Ma \to 0$ on a given triangular mesh, the Roe scheme remains accurate, i.e. flows of arbitrarily small Mach numbers can – at least in principle – be simulated on a fixed triangular mesh. We give an asymptotic analysis of this phenomenon and present a number of numerical results.

1. Introduction

Schemes, originally designed to calculate compressible flow, encounter three problems in low Mach number flow. Firstly, the speeds of acoustic waves and flow phenomena are of different orders of magnitude – their ratio is measured by the Mach number. Low Mach numbers slow down the calculation of phenomena on the time scale of the flow such as heat or water transport (*stiffness problem*). Secondly, the pressure variable has to accommodate a constant background pressure of order $\mathcal{O}(1)$ and the physically relevant pressure variations of order $\mathcal{O}(Ma^2)$, which leads to numerical round-off errors (*cancellation problem*). And thirdly, for stability reasons, upwind schemes introduce artificial viscosity, which depends on the Mach number. In certain settings this can cause the truncation error to be $\mathcal{O}(1/Ma)$, i.e. to grow with decreasing Mach numbers on a given mesh, and thus preventing the numerical solution to approximate inviscid, incompressible flow (*accuracy problem*).

The *cancellation problem* can be avoided by working only with the fluctuation quantities introduced in the wave propagation approach by Leveque [1]. This approach was applied to low Mach number flow by Sesterhenn et al. [2].

To overcome the *stiffness and accuracy problem in steady flow simulations* a variety of time-derivative or flux preconditioning techniques have been developed and applied to compressible (and incompressible) solvers for the inviscid flow

E-mail address: rieper@iau.uni-frankfurt.de

0021-9991/$ - see front matter © 2009 Elsevier Inc. All rights reserved.
doi:10.1016/j.jcp.2009.09.043

equations, such as Turkel's approach, [3,4], or the characteristic time stepping approach by van Leer et al. [5]. The stiffness is reduced by (almost) equalising the propagation speeds of the different waves for $Ma \to 0$, which accelerates the convergence to steady state. At the same time, the artificial viscosity is tuned correctly for all characteristic waves and thus the accuracy problem is circumvented. Preconditioning in the context of viscous flow was dealt with by Choi and Merkle [6]. They report on the absence of the accuracy problem down to $Ma = 10^{-6}$ for their preconditioning methods, which are implemented on grids with quadrilateral cells.

The *accuracy problem for transient flow* was explicitly addressed by Guillard and Viozat [7]. Their asymptotic analysis of the Roe scheme explains the appearance of a pressure term of wrong order as $Ma \to 0$ on *Cartesian grids*. They propose a viscosity–matrix preconditioning to fix the problem.

It is worth mentioning that Discontinuous Galerkin (DG) schemes do not show the accuracy problem as much as finite volume schemes as shown in [8]. Nevertheless, Bassi et al. show that preconditioning improves accuracy and efficiency of DG schemes in the low Mach number regime [9].

Thornber et al. [10] show that there is a one-to-one relation between dissipation of kinetic energy and increase in entropy. Their analysis reveals an unphysical entropy production of Godunov-type schemes at low Mach numbers related to the jumps at the cell interfaces. The aim to minimise these jumps is achieved with an improved reconstruction method presented by Thornber et al. [11]. A fifth-order in space reconstruction is changed in a way so that the jump in the normal component of the velocity in the Riemann problem is reduced. The approach results in a MUSCL scheme capable of calculating low Mach number flows on Cartesian meshes.

Despite the advances attained in the past, simulating low Mach number flows remains a challenge and still has open questions, such as: how to overcome the stiffness while maintaining time accuracy and computing efficiency; and can the reconstruction fix for low Mach number flows presented in [11] be applied to unstructured grids and to second-order reconstructions widely used in practice?

An interesting property of first-order Godunov-type schemes on *triangular meshes* is the absence of these jumps in the normal velocity component. Therefore, these schemes do not show the accuracy problem at low Mach numbers on triangular finite volume cells. This effect is demonstrated and proved with an asymptotic analysis in two dimensions by Rieper and Bader [12], and generalised by Guillard [13].

The failure of certain flux solvers such as HLL even on triangular meshes initiated the analysis presented here. We compare the dissipation rate of the individual characteristic waves for two common flux solvers, Roe and HLL. In general, only a certain class of solvers, which resolve the contact waves explicitly, have Mach-number independent dissipation of the contact wave and are thus able to approximate low Mach number flow. In Section 2 a characteristic analysis is done for the Roe scheme. Section 3 is dedicated to the HLL scheme and a generalisation of the approach for arbitrary flux solvers is given in Section 4. Numerical results corroborating the analysis are given in Section 5.

1.1. Governing equations

The 2D-Euler equations in conservation form are

$$\mathbf{q}_t + \mathbf{f}(\mathbf{q})_x + \mathbf{g}(\mathbf{q})_y = 0,$$

with

$$\mathbf{q} = \begin{bmatrix} \rho \\ \rho u \\ \rho v \\ \rho e \end{bmatrix}, \quad \mathbf{f} = \begin{bmatrix} \rho u \\ \rho u^2 + p \\ \rho u v \\ u(\rho e + p) \end{bmatrix}, \quad \mathbf{g} = \begin{bmatrix} \rho v \\ \rho u v \\ \rho v^2 + p \\ v(\rho e + p) \end{bmatrix},$$

with density ρ, velocity $(u, v)^T$, total specific energy e and pressure p. To close the equations, thermodynamic relations are needed. We use the perfect gas law $p = (\gamma - 1)\rho\varepsilon$, with the adiabatic index γ and $\varepsilon = e - \frac{1}{2}(u^2 + v^2)$ as internal specific energy.

In this study we focus on the one-dimensional behaviour of numerical schemes and therefore assume only plane waves – parallel to the y-axis without loss of generality – so that the 2D-equations collapse to a one-dimensional problem given by

$$\mathbf{q}_t + \mathbf{f}(\mathbf{q})_x = 0. \tag{1.1}$$

Note, that $\mathbf{q}$ and $\mathbf{f}$ still depend on *two* velocity components: the normal velocity u and the transverse velocity v, so that shear waves are possible. In the following we analyse the numerical approximation of this equation and refer to it as the *one-dimensional model case*.

System (1.1) can be (locally) transformed using the right eigenvectors $\mathbf{r}_i$ of the Jacobian $A = \mathrm{d}\mathbf{f}/\,\mathrm{d}\mathbf{q}$ with the transformation matrix $R = [\mathbf{r}_1, \ldots, \mathbf{r}_4]$ and its inverse $R^{-1} = L = [\mathbf{l}_1, \ldots, \mathbf{l}_4]$, to obtain the characteristic form of the Euler equations

$$\frac{\partial \mathbf{w}}{\partial t} + \Lambda \frac{\partial \mathbf{w}}{\partial x} = 0,$$

where the characteristic variables are given by

$$dw_1 = \frac{1}{2a^2}dp - \frac{\rho}{2a}du, \quad \text{(left – running acoustic wave)}$$
$$dw_2 = d\rho - \frac{dp}{a^2}, \quad \text{(entropy wave)}$$
$$dw_3 = \rho dv, \quad \text{(shear wave)}$$
$$dw_4 = \frac{1}{2a^2}dp + \frac{\rho}{2a}du. \quad \text{(right – running acoustic wave)}$$

2. The Roe scheme

The numerical truncation error of an upwind scheme is twofold, originating from temporal and spatial discretisation. In this study we focus only on the numerical dissipation introduced by the flux solver and, therefore, we only study the semi-discrete equations.

2.1. Spatial discretisation

The Roe scheme [14] applied to the *one-dimensional model case* (1.1) can be written in semi-discrete form as

$$\frac{d}{dt}\mathbf{q}_i = -\frac{1}{\Delta x}(\mathbf{f}^{\text{Roe}}_{i+1/2} - \mathbf{f}^{\text{Roe}}_{i-1/2}), \tag{2.2}$$

with the numerical flux function

$$\mathbf{f}^{\text{Roe}}_{i+1/2} = \frac{\mathbf{f}(\mathbf{q}_i) + \mathbf{f}(\mathbf{q}_{i+1})}{2} - \frac{1}{2}|\widehat{A}_{i+1,i}|(\mathbf{q}_{i+1} - \mathbf{q}_i), \tag{2.3}$$

where $\widehat{A}$ denotes the Roe matrix for the right state $\mathbf{q}_{i+1}$ and the left state $\mathbf{q}_i$ of the Riemann problem. Inserting (2.3) into (2.2), we obtain the equations of the semi-discrete Roe scheme:

$$\frac{d}{dt}\mathbf{q}_i = -\frac{\mathbf{f}_{i+1} - \mathbf{f}_{i-1}}{2\Delta x} + \frac{1}{2}\frac{|\widehat{A}_{i+1,i}|(\mathbf{q}_{i+1} - \mathbf{q}_i) - |\widehat{A}_{i,i-1}|(\mathbf{q}_i - \mathbf{q}_{i-1})}{\Delta x}. \tag{2.4}$$

To find the modified equation we expand the first expression on the RHS of (2.4) in a Taylor series

$$\frac{\mathbf{f}_{i+1} - \mathbf{f}_{i-1}}{2\Delta x} = \mathbf{f}_x|_{x_i} + \mathcal{O}(\Delta x^2) = A(\mathbf{q})\mathbf{q}_x|_{x_i} + \mathcal{O}(\Delta x^2),$$

showing the second-order accuracy of the central flux difference. For the second term on the RHS of (2.4) we need an expansion of the Roe matrix. For this purpose we interpret the Roe average $\mathbf{q}_{i+1,i}$ as a deviation $\Delta\mathbf{q}$ of the state $\mathbf{q}_i$

$$\mathbf{q}_{i+1,i} = \mathbf{q}_i + \Delta\mathbf{q},$$

where the Roe average is defined as

$$\mathbf{q}_{i+1,i} = \theta\mathbf{q}_i + (1-\theta)\mathbf{q}_{i+1}, \quad \text{with} \quad \theta = \frac{\sqrt{\rho_i}}{\sqrt{\rho_i} + \sqrt{\rho_{i+1}}}.$$

This can be written in terms of $\mathbf{q}(x,t)$ to obtain

$$\mathbf{q}_{i+1,i} = \theta\mathbf{q}(x_i) + (1-\theta)\mathbf{q}(x_i + \Delta x) = \theta\mathbf{q}(x_i) + (1-\theta)[\mathbf{q}(x_i) + \mathbf{q}_x(x_i)\Delta x + \mathcal{O}(\Delta x^2)] = \mathbf{q}(x_i) + (1-\theta)[\mathbf{q}_x(x_i)\Delta x + \mathcal{O}(\Delta x^2)].$$

The weight θ itself is a function of $\rho(x)$ and can be expanded in a Taylor series about $\rho(x_i)$:

$$\theta(\rho(x_i + \Delta x)) = \theta(\rho(x_i)) + \mathcal{O}(\Delta x) = \frac{1}{2} + \mathcal{O}(\Delta x). \tag{2.5}$$

Using (2.5) we obtain for the Roe average

$$\mathbf{q}_{i+1,i} = \mathbf{q}(x_i) + \left(\frac{1}{2} + \mathcal{O}(\Delta x)\right)(\mathbf{q}_x(x_i)\Delta x + \mathcal{O}(\Delta x^2)) \tag{2.6}$$
$$= \mathbf{q}(x_i) + \frac{1}{2}\mathbf{q}_x(x_i)\Delta x + \mathcal{O}(\Delta x^2), \tag{2.7}$$

so that the deviation $\Delta\mathbf{q}$ between Roe average and inner cell state is

$$\Delta\mathbf{q} = \frac{1}{2}\mathbf{q}_x(x_i)\Delta x + \mathcal{O}(\Delta x^2).$$

The Roe matrix expanded in a Taylor series about $\mathbf{q}_i = \mathbf{q}(x_i)$ is therefore

$$\widehat{A}_{i+1,i} = A(\mathbf{q}_i) + \frac{\partial A}{\partial \mathbf{q}}\Delta\mathbf{q} + \mathcal{O}(\Delta\mathbf{q}^2) = A(\mathbf{q}_i) + \frac{\partial A}{\partial \mathbf{q}}\frac{1}{2}\mathbf{q}_x\Delta x + \mathcal{O}(\Delta\mathbf{q}^2) = A(\mathbf{q}_i) + \mathcal{O}(\Delta x),$$

which gives

$$|\widehat{A}_{i+1,i}| = |A(\mathbf{q}_i)| + \mathcal{O}(\Delta x) \tag{2.8}$$

for the absolute value of the Roe matrix. We can now substitute (2.7) and (2.8) into the viscosity term

$$\eta_{\text{Roe}} := \frac{|\widehat{A}_{i+1,i}|(\mathbf{q}_{i+1} - \mathbf{q}_i) - |\widehat{A}_{i,i-1}|(\mathbf{q}_i - \mathbf{q}_{i-1})}{2\Delta x},$$

to obtain

$$\begin{aligned}\eta_{\text{Roe}} &= \frac{1}{2}(|A(\mathbf{q}_i)| + \mathcal{O}(\Delta x))(\mathbf{q}_x|_{x_{i+1/2}} + \mathcal{O}(\Delta x^2)) - \frac{1}{2}(|A(\mathbf{q}_i)| + \mathcal{O}(\Delta x))(\mathbf{q}_x|_{x_{i-1/2}} + \mathcal{O}(\Delta x^2))\\ &= \frac{1}{2}|A(\mathbf{q}_i)|(\mathbf{q}_x|_{x_{i+1/2}} - \mathbf{q}_x|_{x_{i-1/2}}) + \mathcal{O}(\Delta x)\frac{1}{2}(\mathbf{q}_x|_{x_{i+1/2}} - \mathbf{q}_x|_{x_{i-1/2}}) = \frac{1}{2}|A(\mathbf{q}_i)|\mathbf{q}_{xx}|_{x_i}\Delta x + \mathcal{O}(\Delta x^2).\end{aligned}$$

We can summarise the results in the following modified equation for the semi-discrete Roe scheme:

$$\boxed{\mathbf{q}_t + A(\mathbf{q})\mathbf{q}_x = \tfrac{1}{2}|A(\mathbf{q})|\mathbf{q}_{xx}\Delta x} \tag{2.9}$$

The matrix on the right hand side is called viscosity matrix of the Roe scheme $V_{\text{Roe}} = |A(\mathbf{q})|$ in analogy to the viscosity terms in the Navier–Stokes equation. Note that, by derivation, the Roe scheme satisfies this equation to second order accuracy, see also Kröner [15].

2.2. Characteristic form

Why is it absolutely essential to work in characteristic variables? Simply said, because, for hyperbolic equations, information travels along characteristics and upwind schemes (should) add artificial viscosity on the characteristic variables *according to the characteristic speeds*. The pressure, for example, is transported with flow velocity u in an entropy wave and, in this wave, it should be damped proportional to $|u| = \mathcal{O}(1)$. In an acoustic wave, however, the pressure is transported with the sound speed a and should be damped proportional to $|a| = \mathcal{O}(1/Ma)$. If we consider the transport of pressure as a whole, i.e. in the primitive form of the equations, we are not able to see, which part of the pressure belongs to an entropy, and which to an acoustic wave and, consequently, we cannot assess whether the corresponding damping is of the right order of magnitude. For this reason, we want to analyse the artificial viscosity on the individual characteristic waves and derive the characteristic form of the modified equation.

Let $\mathbf{r}_1, \ldots, \mathbf{r}_4$ be the right eigenvectors of the Jacobian $A = \mathrm{d}\mathbf{f}/\mathrm{d}\mathbf{q}$ at the state $\mathbf{q}(x,t)$ with the eigenvalues

$$\lambda_1 = u - a, \quad \lambda_2 = u, \quad \lambda_3 = u, \quad \lambda_4 = u + a.$$

We apply the transformation matrices $R = [\mathbf{r}_1, \ldots, \mathbf{r}_4]^T$ and R^{-1} to the modified Eq. (2.9)

$$R^{-1}\mathbf{q}_t + (R^{-1}AR)R^{-1}\mathbf{q}_x = \frac{1}{2}(R^{-1}|A|R)R^{-1}\mathbf{q}_{xx}\Delta x$$

and, using the relations $|A| = R|\Lambda|R^{-1}$ and $\mathrm{d}\mathbf{w} = R^{-1}\mathrm{d}\mathbf{q}$, we obtain the modified equation in characteristic variables

$$\frac{\partial}{\partial t}w_k + \lambda_k\frac{\partial}{\partial x}w_k = \frac{1}{2}|\lambda_k|\frac{\partial^2}{\partial x^2}w_k\Delta x. \tag{2.10}$$

We want to compare the magnitudes of *physical* convection with *artificial* dissipation given by the truncation error on the RHS of (2.10). For this purpose we scale the equation with $|\lambda_k|$, so that the convection term is $\mathcal{O}(1)$:

$$\frac{1}{|\lambda_k|}\frac{\partial}{\partial t}w_k + \sigma_k\frac{\partial}{\partial x}w_k = \frac{1}{2}\frac{\partial^2}{\partial x^2}w_k\Delta x, \tag{2.11}$$

where $\sigma_k = \lambda_k/|\lambda_k| = \pm 1$, depending on the sign of the propagation velocity. Interestingly, the truncation error *for all characteristic waves*,

$$\tau_k = \frac{1}{2}\frac{\partial^2}{\partial x^2}w_k\Delta x = \mathcal{O}(\Delta x), \tag{2.12}$$

is independent of Ma as $Ma \to 0$. We therefore conclude: the one-dimensional analysis of the dissipative behaviour of the Roe scheme indicates that the accuracy, given by the truncation error, is independent of the Mach number. If it were not for the cancellation error due to round-off, the Roe scheme could calculate (with a constant accuracy) flows on a fixed mesh at any Mach number, no matter how small.

2.3. Temporal discretisation

Thornber et al. show in Ref. [10] with numerical experiments that a change of order of the temporal discretisation has no influence on the dissipation rate of kinetic energy for decreasing Mach numbers. Indeed in [16] the author shows that an explicit first-order temporal discretisation of the Roe scheme does not affect the Mach-number independence of the truncation error. This can be seen from the fully-discrete modified equation for a characteristic wave w given by

$$\frac{\partial}{\partial t}w + \lambda\frac{\partial}{\partial x}w = \frac{1}{2}|\lambda|\Delta x(1-c)\frac{\partial^2}{\partial x^2}w, \tag{2.13}$$

with corresponding CFL number $c = \lambda\Delta t/\Delta x$. This is analogous to the modified equation of the standard upwind method for the linear wave equation derived in [1]. Due to the small time steps $\Delta t = \mathcal{O}(Ma)$ the CFL number for the entropy or shear wave also satisfies

$$c_{\text{contact}} = \mathcal{O}(Ma),$$

so $1 - c_{\text{contact}} \approx 1$ and the additional factor in (2.13) compared to the semi-discrete modified Eq. (2.11) disappears. This explains why the dissipation rate for contact waves is not notably influenced by the temporal discretisation for decreasing Mach numbers. The same argument holds for other flux solvers so that we restrict ourselves to a semi-discrete analysis in the following.

3. The HLL scheme

In this section we analyse the behaviour of the two-wave Riemann solver by Harten, Lax and van Leer (HLL) [17] in the low Mach number regime for the one-dimensional model case. HLL is known for its dissipative behaviour but, for the first time, asymptotic expressions for the dissipation terms in characteristic variables for $Ma \to 0$ are derived here.

3.1. Spatial discretisation

The first-order HLL scheme in semi-discrete form is given by

$$\frac{\mathrm{d}}{\mathrm{d}t}\mathbf{q}_i = -\frac{1}{\Delta x}(\mathbf{f}^{\text{HLL}}_{i+1/2} - \mathbf{f}^{\text{HLL}}_{i-1/2}),$$

with the numerical flux function as given in [18,19]

$$\mathbf{f}_{\text{HLL}}(\mathbf{q}_{\text{R}}, \mathbf{q}_{\text{L}}) = \frac{\mathbf{f}(\mathbf{q}_{\text{R}}) + \mathbf{f}(\mathbf{q}_{\text{L}})}{2} - \frac{1}{2}\frac{S_{\text{R}} + S_{\text{L}}}{S_{\text{R}} - S_{\text{L}}}(\mathbf{f}(\mathbf{q}_{\text{R}}) - \mathbf{f}(\mathbf{q}_{\text{L}})) + \frac{S_{\text{R}}S_{\text{L}}}{S_{\text{R}} - S_{\text{L}}}(\mathbf{q}_{\text{R}} - \mathbf{q}_{\text{L}}), \tag{3.14}$$

under the assumption that

$$S_{\text{L}} \leqslant 0 \leqslant S_{\text{R}}, \quad S_{\text{L}} \neq S_{\text{R}},$$

which is justified in the low Mach number regime. Here S_{L} and S_{R} are wave speeds that are faster than the left- and right-running signal speeds in the underlying Riemann problem and have to be estimated adequately. If there is a Roe-Matrix $\widehat{A} = \widehat{A}(\mathbf{q}_{\text{R}}, \mathbf{q}_{\text{L}})$ for this Riemann problem we can write $\mathbf{f}(\mathbf{q}_{\text{R}}) - \mathbf{f}(\mathbf{q}_{\text{L}}) = \widehat{A}(\mathbf{q}_{\text{R}} - \mathbf{q}_{\text{L}})$. Substituting this into Eq. (3.14) we obtain

$$\mathbf{f}_{\text{HLL}}(\mathbf{q}_{\text{R}}, \mathbf{q}_{\text{L}}) = \frac{\mathbf{f}(\mathbf{q}_{\text{R}}) + \mathbf{f}(\mathbf{q}_{\text{L}})}{2} - \frac{1}{2}\frac{S_{\text{R}} + S_{\text{L}}}{S_{\text{R}} - S_{\text{L}}}\widehat{A}(\mathbf{q}_{\text{R}} - \mathbf{q}_{\text{L}}) + \frac{S_{\text{R}}S_{\text{L}}}{S_{\text{R}} - S_{\text{L}}}(\mathbf{q}_{\text{R}} - \mathbf{q}_{\text{L}})$$

for the numerical flux of the HLL scheme. We assume $\mathbf{q}(x,t)$ to be a smooth function. Following the approach of Section 2 we obtain for the modified equation of the HLL scheme:

$$\mathbf{q}_t + A\mathbf{q}_x = \frac{1}{2}V_{\text{HLL}}\mathbf{q}_{xx}\Delta x,$$

where

$$V_{\text{HLL}} = \frac{S_{\text{R}} + S_{\text{L}}}{S_{\text{R}} - S_{\text{L}}}|A(\mathbf{q})| - 2\frac{S_{\text{R}}S_{\text{L}}}{S_{\text{R}} - S_{\text{L}}}I + \mathcal{O}(\Delta x)$$

is the viscosity matrix of the HLL scheme with the Jacobian $A(\mathbf{q})$ and the identity matrix I as presented in [18,19].

3.2. Characteristic form

The viscosity matrix V_{HLL} has the same eigenvectors $\mathbf{r}_1, \ldots, \mathbf{r}_4$ as the Jacobian $A = \mathrm{d}\mathbf{f}/\mathrm{d}\mathbf{q}$, so that we can transform the modified equation using $R = [\mathbf{r}_1, \ldots, \mathbf{r}_4]$

$$R^{-1}\mathbf{q}_t + (R^{-1}AR)R^{-1}\mathbf{q}_x = \frac{1}{2}(R^{-1}V_{\text{HLL}}R)R^{-1}\mathbf{q}_{xx}\Delta x,$$

into a (locally) decoupled system with the characteristic variables $d\mathbf{w} = R^{-1}d\mathbf{q}$:

$$\mathbf{w}_t + \Lambda \mathbf{w}_x = \frac{1}{2}\Lambda_{\mathrm{HLL}}\mathbf{w}_{xx}\Delta x, \tag{3.15}$$

where $\Lambda = \mathrm{diag}(u-a, u, u, u+a)$ is the matrix of eigenvalues and

$$\Lambda_{\mathrm{HLL}} = R^{-1}\left(\underbrace{\frac{S_R+S_L}{S_R-S_L}}_{\alpha}|A| - \underbrace{2\frac{S_R S_L}{S_R-S_L}}_{\delta} I\right)R \tag{3.16}$$

is the characteristic form of the viscosity matrix V_{HLL}. It can be simplified using the relation $|A| = R|\Lambda|R^{-1}$ and the identity $R^{-1}IR = I$ to obtain

$$\Lambda_{\mathrm{HLL}} = \alpha|\Lambda| - \delta I = \mathrm{diag}(\alpha|u-a| - \delta, \alpha|u| - \delta, \alpha|u| - \delta, \alpha|u+a| - \delta) =: \mathrm{diag}(\mu_1, \ldots, \mu_4),$$

where the μ_i can be interpreted as *numerical viscosity coefficients* for the individual characteristic waves. In many implementations of the HLL scheme the wave speeds satisfy the asymptotic equalities

$$S_R \sim u + a$$
$$S_L \sim u - a$$

where $\sim$ has the meaning *asymptotically equal*, i.e. their ratio converges to a constant for $Ma \to 0$. With this assumption we find for α

$$\alpha = \frac{S_R+S_L}{S_R-S_L} \sim \frac{2u}{2a} = Ma \tag{3.17}$$

and for δ

$$\delta = 2\frac{S_R S_L}{S_R - S_L} \sim \frac{(u-a)(u+a)}{a},$$

which can be written as

$$\delta \sim (Ma-1)(u+a) \tag{3.18a}$$

or equivalently as

$$\delta \sim (Ma+1)(u-a). \tag{3.18b}$$

The coefficient of artificial viscosity μ_1 for the *left-running acoustic wave* satisfies

$$\mu_1 = \alpha|u-a| - \delta \sim Ma|u-a| - (u-a)(Ma+1) \sim (2Ma+1)(a-u). \tag{3.19}$$

Eq. (3.15) can be written in a form, where the convective part is scaled to $\mathcal{O}(1)$ for each individual characteristic wave:

$$\frac{1}{|\lambda_i|}\frac{\partial}{\partial t}w_i + \sigma_i\frac{\partial}{\partial x}w_i = \frac{1}{2}\frac{\mu_i}{|\lambda_i|}\frac{\partial^2}{\partial x^2}w_i\Delta x, \tag{3.20}$$

where again $\sigma_i = \lambda_i/|\lambda_i| = \pm 1$. The truncation error for the left-running acoustic wave w_1 is given by

$$\tau_1 = \frac{1}{2}\frac{\mu_1}{|\lambda_1|}\frac{\partial^2}{\partial x^2}w_1\Delta x. \tag{3.21}$$

Using the fact that $|\lambda_1| = |u-a| = a-u$ for $Ma < 1$, and inserting (3.19) in (3.21), this can be simplified to

$$\tau_1 = \frac{1}{2}(2Ma+1)\frac{\partial^2}{\partial x^2}w_1\Delta x = \mathcal{O}(\Delta x) \quad \text{as} \quad Ma \to 0, \Delta x \to 0. \tag{3.22}$$

The analogous is true for the truncation error of the right-running acoustic wave, τ_4. Eq. (3.22) implies: the HLL scheme resolves acoustic waves accurately for $Ma \to 0$.

For contact and shear waves, with $|\lambda_{2,3}| = |u|$, the coefficient of artificial viscosity is

$$\mu_{2,3} = \alpha|u| - \delta \sim Ma|u| - (Ma-1)(u+a),$$

so that we obtain for the truncation error $\tau_2 = \tau_3$:

$$\begin{aligned}\tau_2 &= \frac{1}{2}\frac{\mu_2}{|\lambda_2|}\frac{\partial^2}{\partial x^2}w_2\Delta x = \frac{1}{2}\frac{Ma|u| - (Ma-1)(u+a)}{|u|}\frac{\partial^2}{\partial x^2}w_2\Delta x = \frac{1}{2}\left\{Ma - (Ma-1)(\pm 1 + \frac{1}{Ma}\right\}\frac{\partial^2}{\partial x^2}w_2\Delta x \\ &\sim \frac{1}{2}\frac{\partial^2}{\partial x^2}w_2\frac{\Delta x}{Ma} = \mathcal{O}\left(\frac{\Delta x}{Ma}\right) \quad \text{as} \quad Ma \to 0.\end{aligned} \tag{3.23}$$

Compared to the physical transport, scaled to $\mathcal{O}(1)$, the truncation error, and with it the artificial dissipation, increases like $1/Ma$ for $Ma \to 0$. This behaviour occurs equally for entropy and shear waves and explains the massive loss of accuracy for low Mach number calculations with the HLL scheme.

4. Generalisation

The analysis presented is limited to specific flux solvers such as Roe and HLL because the matrix of artificial viscosity and the Jacobian can be diagonalised simultaneously so that the dissipation of each characteristic wave becomes evident. Most schemes do not have this property making a diagonalisation unfeasible. With the following trick a full diagonalisation can be circumvented: we insert into the flux difference a single characteristic wave and obtain a modified equation for this characteristic. To analyse the dissipative behaviour on a *shear wave* we let the following quantities constant:

$$u = \text{const}, \qquad p = \text{const}, \qquad \rho = \text{const},$$

only the transverse velocity v is allowed to change between neighbouring cells, i.e.: $v_i \neq v_{i+1}$.

In a similar fashion, a special entropy wave – given by a density jump – can be analysed. The flux solver should be analysed with constant data

$$u, v = \text{const}, \quad p = \text{const}$$

and a density ρ which is allowed to jump: $\rho_i \neq \rho_{i+1}$.

Using this analysis it was shown in [16] that HLLC and AUSM dissipate shear waves independently of the Mach number. The flux vector splittings by van Leer and Steger–Warming have a dissipation rate proportional to 1/Ma leading to a failure of these schemes for low Mach number flows.

5. Numerical results

5.1. One-dimensional flow

A one-dimensional analysis is, of course, best verified with one-dimensional experiments. Our goal is to visualise the dissipative behaviour on simple waves, i.e. with a jump in a single characteristic, for various Mach numbers $Ma = 10^{-1}, 10^{-2}$ and 10^{-3}. The Mach numbers are enforced by adapting the flow velocity according to $u = aMa = \sqrt{\gamma p/\rho}Ma$, while keeping the background pressure p_0 and density ρ_0 constant. The adiabatic index γ is set to 1.4 throughout our calculations. Forward Euler in time is used but an implicit method could be used as well. The calculations are stopped after the signal has passed 0.1 of the flow domain [0,1]. At the boundary we use Neumann boundary conditions.

5.1.1. Entropy wave

We set up a simple entropy wave with an initial density jump at $t_0 = 0$, given by $\rho(x < 0.5) = 1.0$ and $\rho(x \geqslant 0.5) = 0.5$, see Fig. 1. Note that for the signal to pass $\Delta x = 0.1$ the number of time steps Δt increases for lower Mach numbers and, at the same time, the size of Δt decreases. For HLL, in agreement with (3.23), the dissipation of the signal increases with lower Mach numbers. For $Ma = 10^{-3}$ the signal is completely smeared out. Shown in the right of Fig. 1 is the result for the Roe scheme. In agreement with (2.12), the dissipation is independent of the Mach number.

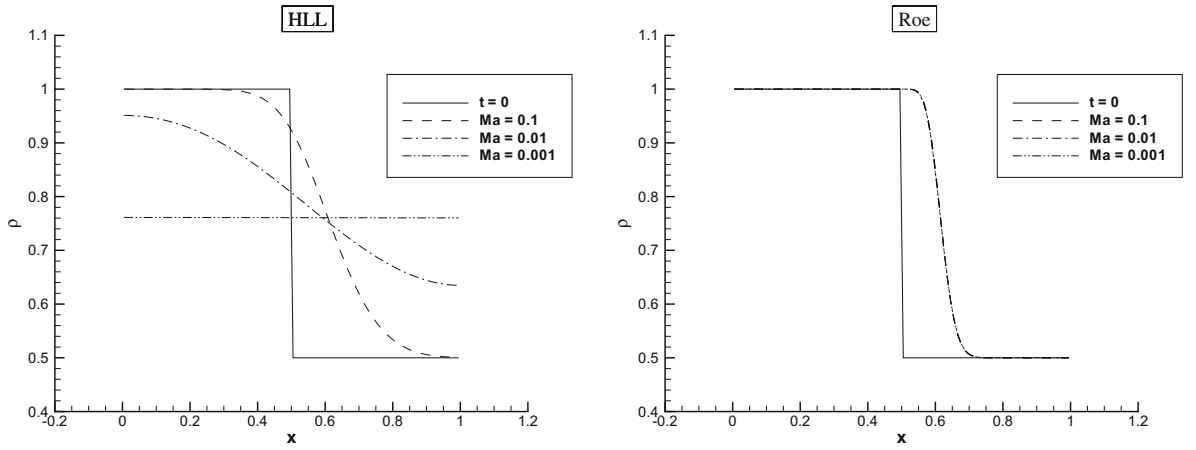

Fig. 1. Dissipation of a density jump. Left (HLL): The smearing strongly depends on the Mach number. Right (Roe scheme): the smearing is small and independent of the Mach number.

5.1.2. Shear wave

In view of two-dimensional flow, we introduce a transversal velocity component v into the flux solvers but maintain the one-dimensional setting. For the shear wave we set $v(x < 0.5) = u_{\text{ref}} = \sqrt{\gamma}Ma$ and $v(x \geqslant 0.5) = 0.5u_{\text{ref}} = 0.5\sqrt{\gamma}Ma$. In Fig. 2 the velocity is scaled by u_{ref} to fit all data into a single diagram. The results are completely analogous to the entropy wave, again in agreement with the analysis.

5.1.3. Acoustic wave

We set up a left- and a right-running acoustic wave with an initial jump of the 'normal' velocity u given by $u(x < 0.5) = u_{\text{ref}} = \sqrt{\gamma}Ma$ and $u(x \geqslant 0.5) = 0.9u_{\text{ref}}$, see Fig. 3. The pressure pulse is expected to be $\mathcal{O}(Ma)$, therefore we plot $(p - p_0)/Ma$. The exact solution is a quasi linear acoustic pulse. The dissipation of the signal by HLL and Roe is independent of the Mach number, which agrees with (3.22) and (2.12), respectively.

5.2. Two-dimensional flow

In [12] the authors have shown, that a prerequisite for an upwind scheme to well approximate low Mach number flow is the use of triangular finite volume cells – no matter whether the grid is structured or unstructured. We therefore compare the behaviour of HLL and Roe scheme on a triangular grid and investigate how the numerical Reynolds numbers affect two-dimensional flow.

5.2.1. Potential versus creeping flow

We use the flow around a cylinder as test case since an incompressible potential flow solution is known, i.e. we have an analytical reference solution for $Ma \to 0$. The *initial conditions* are set uniform to $\rho_0 = 1.0,\ \mathbf{u}_0 = (u_0, 0)^T,\ p_0 = 1.0$, where the absolute value $\|\mathbf{u}_0\| = \sqrt{\gamma}Ma_0$ of the initial velocity is set to meet the prescribed initial Mach number Ma_0, and γ is the adiabatic index set to 1.4 throughout our calculations. The exact solution at infinity is assumed uniform

$$\rho_\infty = 1.0, \quad \mathbf{u}_\infty = (u_\infty, 0)^T, \quad p_\infty = 1.0.$$

In the *far-field boundary conditions* this solution is assumed to be a good approximation of the solution at the outer boundary. These values are prescribed in the ghost cells.

For the body-fitted, unstructured grid we use about $n_\phi = 150$ cells along the circumference and 10.000 in total. For the boundary at the cylinder surface we use *solid wall boundary conditions*, i.e. we copy all (primitive) variable values from the outer most cells into the neighbouring ghost cells, except for u which, in addition, gets the opposite sign in the ghost cell. We use an explicit forward Euler, which turns out to be rather efficient, compare Section 5.2.5. Any implicit scheme could be used with increasing time step sizes to accelerate the convergence to steady state.

In Fig. 4 we see the contour lines of the dynamic pressure $p_{\text{dyn}} = p - p_0$ for an inflow Mach number of $M = 10^{-6}$. The first-order Roe scheme (top right) approximates ideal potential flow (top left) very well concerning the absolute value of the pressure as well as the distribution of the isolines with the typical $\cos^2$-characteristic: two stagnation points with high-pressure and two low-pressure regions above and under the profile.

The first-order HLL scheme produces a pressure field (bottom right) that is about 10^5 times too large and has a cosine-characteristic: an high-pressure region in the front and a low-pressure region in the wake of the profile. For comparison, an analytical solution to *creeping or Stokes flow* is presented at the bottom of Fig. 4.

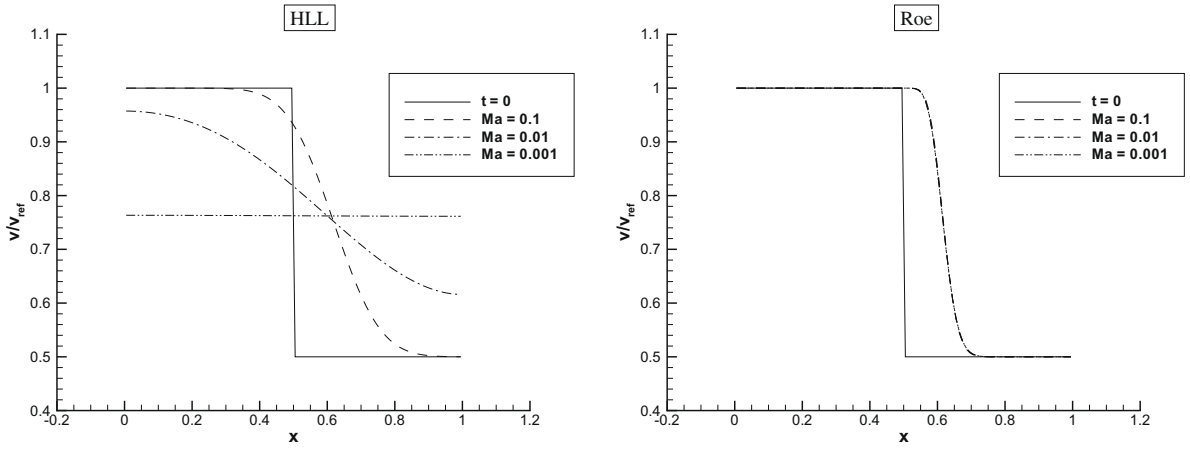

Fig. 2. Dissipation of a jump in the transversal velocity v. Left (HLL): The smearing strongly depends on the Mach number. Right (Roe scheme): the smearing is small and independent of the Mach number.

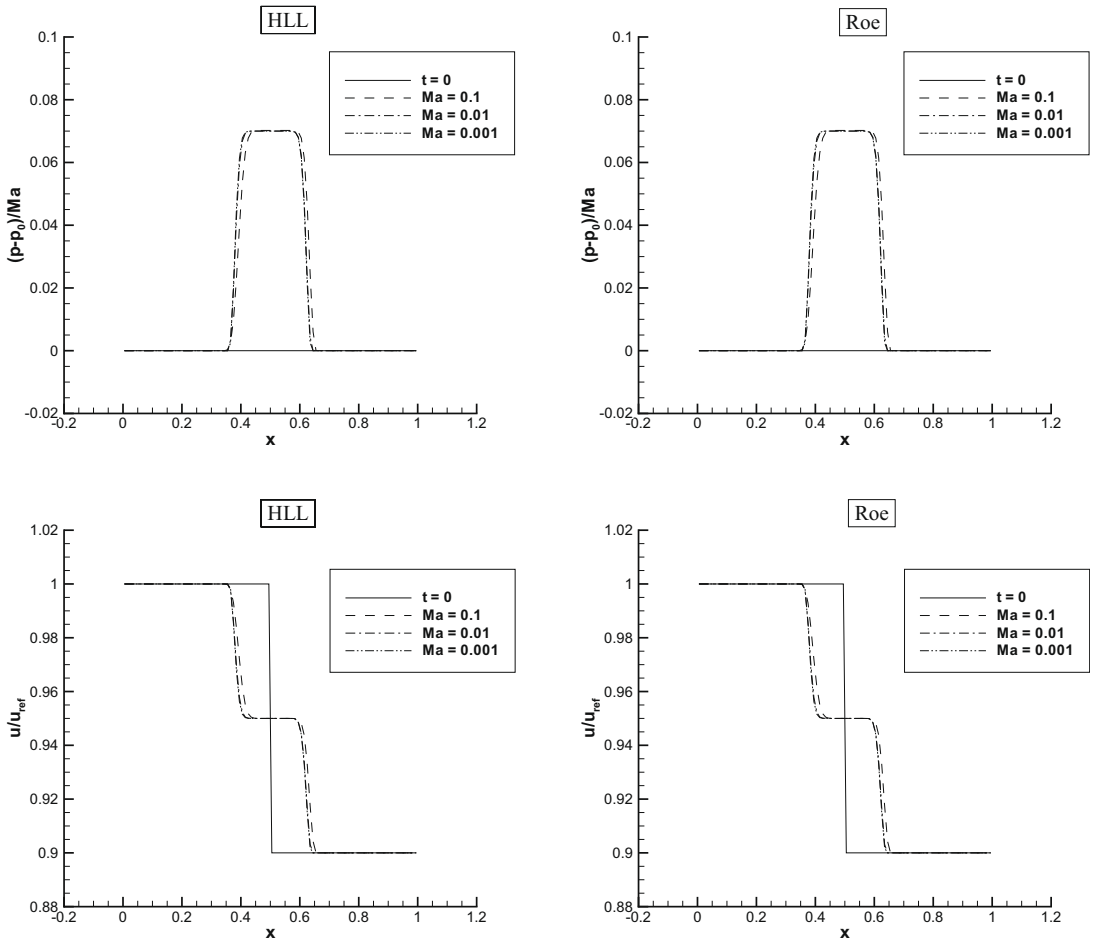

Fig. 3. Dissipation of an acoustic wave.

5.2.2. Numerical Reynolds number

The astonishing resemblance between Stokes flow and HLL at low Mach numbers suggests the following analogy: Stokes flow is characterised by a vanishing Reynolds number, $\mathrm{Re} \approx 0$, which is defined as

$$Re = \frac{\text{magnitude of convection}}{\text{magnitude of viscosity}}. \tag{5.24}$$

There is no *physical* viscosity in the Euler equations but, as truncation error in the modified equations, there is *artificial* viscosity, which can be compared to the convection of the *characteristic variables*. We therefore define the numerical Reynolds number for the various characteristic quantities as

$$Re_{\mathrm{num}} = \frac{\text{magnitude of convection}}{\text{magnitude of the truncation error}}. \tag{5.25}$$

Interestingly, the numerical Reynolds number is $\mathcal{O}(1/\Delta x)$ for all characteristic waves for the Roe scheme and for the acoustic waves for HLL. Thus, for $\Delta x = \text{const}$ we obtain $\mathrm{Re}_{\mathrm{num}} = \text{const}$ as $Ma \to 0$, i.e. a weakly dissipative behaviour of the scheme, depending on the (fixed) resolution. In contrast, shear and entropy waves in the HLL scheme are characterised by $Re_{\mathrm{num}} = \mathcal{O}(Ma/\Delta x)$, i.e. on a fixed mesh and decreasing Mach number $Re_{\mathrm{num}} \to 0$, which is highly viscous – comparable to Stokes flow of fluids like honey or tar.

5.2.3. Magnitude of pressure fluctuations

In the literature [7,20] it is stated that upwind schemes *can* produce pressure fluctuations

$$p_{\mathrm{fluc}} = \frac{p_{\max} - p_{\min}}{p_0} \tag{5.26}$$

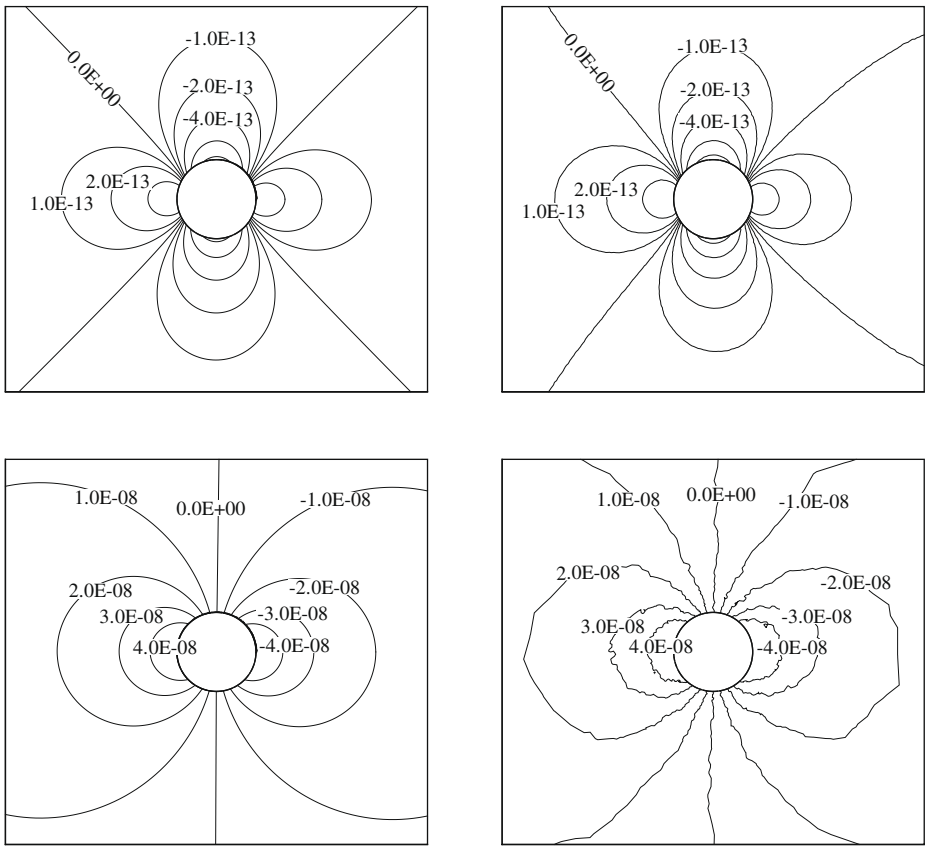

Fig. 4. Isovalues of pressure for potential flow (top left), the Roe scheme (top right), creeping flow (bottom left) and the HLL scheme (bottom right) for $Ma = 10^{-6}$.

of the wrong order $\mathcal{O}(Ma)$. We have given a criterion for this failing behaviour in [12] (triangular finite volume cells) as well as in this paper and present some numerical evidence. In Fig. 5 the pressure fluctuations for Mach numbers from $Ma = 10^{-1}$ down to $Ma = 10^{-7}$ for the first-order Roe (left) and HLL scheme (right) are shown. The results were obtained for a cylinder and a NACA0012 grid, both with about 10.000 grid cells. The pressure field produced by the Roe scheme is directly linked to the kinetic energy (Bernoulli's Principle) and consequently is proportional to Ma^2. The HLL scheme produces pressure fluctuations that are $\mathcal{O}(Ma)$ – in analogy to Stokes flow, where the pressure field originates in viscous forces that are proportional

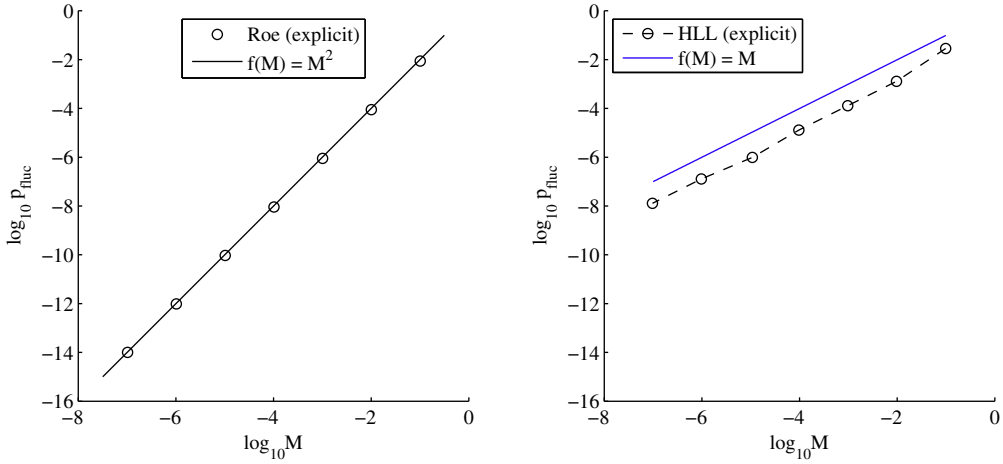

Fig. 5. Pressure fluctuations for various Mach number for Roe (left) and HLL (right).

to the velocity, i.e. the inflow Mach number. These diagrams were validated for grids with 300 up to half a million cells without qualitative change of p-Ma-dependency.

5.2.4. Entropy transport

In ideal subsonic flow there is no entropy production, but numerical dissipation of momentum creates entropy in the solution – predominantly in shear layers near the stagnation points. The amount of entropy produced is therefore a measure for the dissipative behaviour of the numerical scheme. In Fig. 6 the entropy distributions in the steady state – both fields with the same scaling – are given for the first-order Roe (left) and HLL scheme (right). Comparing the magnitude of entropy confirms that the Roe scheme is less dissipative; but more importantly: the Roe scheme maintains its convective or upwind character while the HLL scheme transports the entropy isotropically as in heat conduction. This numerical dissipation-dominated transport has its physical counterpart in creeping flow, where the convective terms are neglected. This also agrees with the notion of numerical Reynolds number: $Re_{\text{num}} \to 0$ for $Ma \to 0$ for the entropy wave in the HLL scheme.

5.2.5. Efficiency study

There is no doubt that phenomena on the time scale of the flow, such as the transport of entropy, humidity or a chemical substance are practically frozen with an explicit upwind scheme in low Mach number flow, since the number of time steps needed increases like $\mathcal{O}(1/Ma)$. In this case a preconditioning technique as proposed by Turkel [3] or van Leer et al. [5] is indispensable.

On the other hand, acoustic phenomena are calculated in $\mathcal{O}(1)$ time steps. Interestingly, the adaption of the flow field to a perturbation such as a moving obstacle happens on the acoustic time scale. The following numerical experiment serves to measure the time from the sudden onset of fluid motion (uniform initial conditions) to the steady state. Once the acoustic waves have left the domain, a steady pressure field settles around the cylinder. The passed CPU time (Pentium 4 with

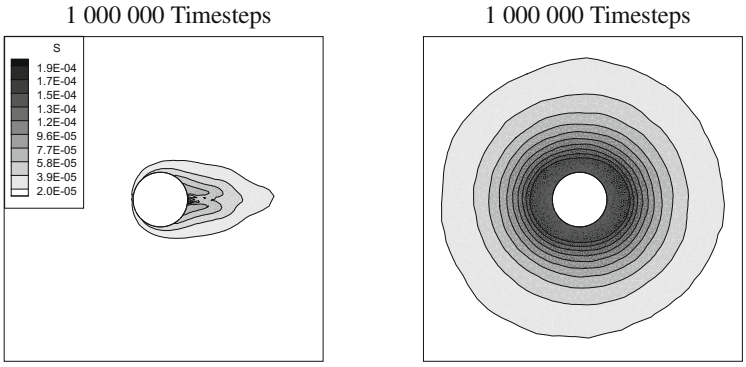

Fig. 6. Entropy isolines for Roe (left) and HLL at $M = 10^{-3}$ with the same scaling.

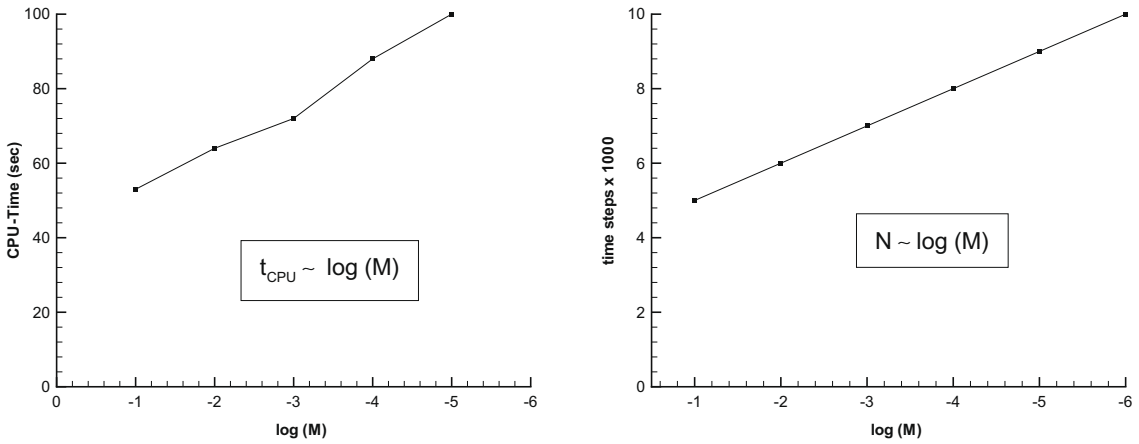

Fig. 7. Efficiency study for the flow around a cylinder (150×50 triangular cells) with the explicit first-order Roe scheme on a Pentium 4 with 3.0 GHz. CPU time (left) and number of explicit time steps (right) for convergence to steady state from homogeneous initial conditions. The pressure field settles to steady state after $\mathcal{O}(\log(Ma))$ time steps.

3.0 GHz) till convergence is presented in the left of Fig. 7. On the right, a similar diagram shows the number of time steps needed. Interestingly, the time for the pressure field to settle down is of the order of the logarithm of the Mach number:

$$t_{\mathrm{CPU}} = \mathcal{O}(\log Ma_0).$$

For the class of exterior low Mach number flows around obstacles, such as aerofoils, a standard upwind scheme on a triangular grid (primary cells) is rather efficient. We do not have similar studies for preconditioned implicit or explicit methods, but it would be interesting to see, whether the classical Roe scheme on triangular cells is competitive. Note, that already for $Ma \approx 0.1$ the flow behaves practically incompressible, see for example [21].

6. Conclusion

We have shown with a one-dimensional analysis that the right amount of artificial viscosity on each individual characteristic variable is a prerequisite for an upwind scheme to approximate low Mach number flow. For this purpose we introduced the notion of *numerical Reynolds number of characteristic variables* and showed the usefulness of this analogy with a number of numerical experiments. The results encourage the use of the standard first-order Roe scheme on triangular grid cells for moderately low Mach numbers. The relation $t_{CPU} = \log(Ma)$ indicates unexpectedly good efficiency for *explicit* schemes.

We are aware that the results on their own are rather theoretical, since in practice higher-order schemes, at least of order 2, are common. The question, therefore, is, how can the results presented in this analysis be applied to practical applications. It is known that for low Mach number flows, Riemann solvers and reconstruction methods cannot be considered separately, but the interplay between them has to be taken into account – both have to satisfy certain properties. While our analysis has shown that only certain upwind schemes resolving all characteristic waves are suitable for low Mach number flows, the analysis presented in [11] made clear that the reconstruction has to be fixed to allow Riemann solvers to produce the right amount of entropy in low Mach number flow simulation.

Acknowledgments

I want to thank my PhD thesis advisor Prof. Dr. Georg Bader for his support of my work. Special thanks to Dr. Sabine Roller for supporting my usage of the HYDSOL code and for raising my interest in the field of low Mach number flow. Thanks also to Dr. Friedemann Kemm for the fruitful discussions.

References

[1] R.J. Leveque, Finite volume methods for hyperbolic problems, Cambridge Texts in Applied Mathematics, Cambridge University Press, Cambridge, 2002.
[2] J. Sesterhenn, B. Müller, H. Thomann, On the cancellation problem in calculating compressible low Mach number flows, J. Comput. Phys. 151 (2) (1999) 597–615.
[3] E. Turkel, Preconditioned methods for solving the incompressible and low speed compressible equations, J. Comput. Phys. 72 (1987) 277–298.
[4] E. Turkel, A. Fiterman, B. van Leer, Frontiers of computational fluid dynamics 1994, CMAS: Computational Methods in Applied Sciences, Chapter. Preconditioning and the Limit of the Compressible to the Incompressible Flow Equations for Finite Difference Schemes, Wiley, Chichester, 1995.
[5] B. van Leer, W.-T. Lee, P. Roe, Characteristic Time-stepping or Local Preconditioning of the Euler Equations, AIAA Paper 91-1552, 1991.
[6] Y.-H. Choi, C. Merkle, The application of preconditioning in viscous flows, J. Comput. Phys. 105 (2) (1993) 207–223.
[7] H. Guillard, C. Viozat, On the behaviour of upwind schemes in the low Mach number limit, Comput. Fluids 28 (1) (1999) 63–86.
[8] M. Feistauer, V. Kučera, On a robust discontinuous Galerkin technique for the solution of compressible flow, J. Comput. Phys. 224 (1) (2007) 208–221.
[9] F. Bassi, C. De Bartolo, R. Hartmann, A. Nigro, A discontinuous Galerkin method for inviscid low Mach number flows, J. Comput. Phys. 228 (11) (2009) 3996–4011.
[10] B. Thornber, D. Drikakis, R. Williams, D. Youngs, On entropy generation and dissipation of kinetic energy in high-resolution shock-capturing schemes, J. Comput. Phys. 227 (10) (2008) 4853–4872.
[11] B. Thornber, A. Mosedale, D. Drikakis, D. Youngs, R. Williams, An improved reconstruction method for compressible flows with low Mach number features, J. Comput. Phys. 227 (10) (2008) 4873–4894.
[12] F. Rieper, G. Bader, The influence of cell geometry on the accuracy of upwind schemes in the low Mach number regime, J. Comput. Phys. (2009).
[13] H. Guillard, On the behavior of upwind schemes in the low Mach number limit. IV: P0 Approximation on triangular and tetrahedral cells, Comput. Fluids 38 (10) (2009) 1969–1972.
[14] P. Roe, Approximate Riemann solvers, parameter vectors, and difference schemes, J. Comput. Phys. 43 (1981) 357–372.
[15] D. Kröner, Numerical schemes for conservation laws, Wiley–Teubner Series Advances in Numerical Mathematics, Wiley, Teubner, Chichester, Stuttgart, 1997.
[16] F. Rieper, On the Behaviour of Numerical Schemes in the Low Mach Number Regime, Ph.D. Thesis, Brandenburg Technical University, Cottbus, 2008.
[17] A. Harten, P.D. Lax, B. van Leer, On upstream differencing and Godunov-type schemes for hyperbolic conservation laws, SIAM Rev. 25 (1983) 35–61.
[18] B. Einfeldt, On Godunov-type methods for gas dynamics, SIAM J. Numer. Anal. 25 (2) (1988) 294–318.
[19] F. Kemm, Carbuncle-freie Flußberechnungen auf der Basis von HLLE und HLLEM, Tech. Rep., Brandenburgische Technische Universität Cottbus, 2004.
[20] A. Meister, Analyse und Anwendung Asymptotik-basierter numerischer Verfahren zur Simulation reibungsbehafteter Strömungen in allen Mach-Zahlbereichen, Habilitationsschrift, Universität Hamburg, 2001.
[21] G. Volpe, Performance of compressible flow codes at low Mach numbers, AIAA J. 31 (1) (1993) 49–56.